Geophysical investigation of a mineral (salt) water aquifer in Turkey

ISSN 1431-2174, Volume 18, Number 5

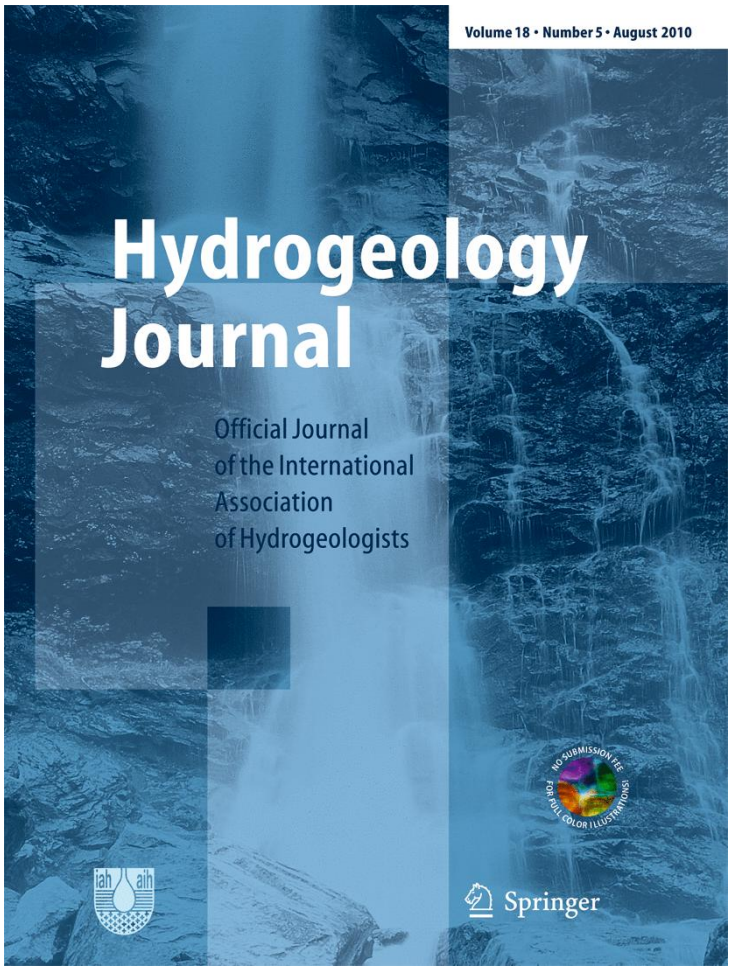

Geophysical investigation of a mineral groundwater resource in Turkey

Daniele Boiero · Alberto Godio · Mario Naldi · Ercan Yigit

Abstract The hydrogeological conditions in Uludag (Nilufer River catchment, Bursa, Turkey) were assessed, using time-domain electromagnetic soundings, electrical resistivity and induced polarisation tomography, to detect the most promising zones for new water-well siting, in order to increase the quantity of water for bottling. The hydrogeological model is quite complex: deep mineral and thermal water rises from a main vertical fault which separates two lithological complexes. The highly mineralised (deep) water is naturally mixed with low mineralised water at a shallow depth, 30–40m; the mixed mineral water is found in some surface springs and shallow wells, while the highly mineralised water is found at depth in some unused deep wells located close to the main fault. All the water points (springs and wells) are located inside a "mineral water belt" on the north side of the Nilufer River. The geophysical survey confirmed the hydrogeological model and highlighted four promising zones for well siting (zones with very low electrical resistivity and high induced polarisation anomalies, corresponding to the main water-bearing faults). One of the geophysical anomalies, the furthest from the exploited sources, was verified by means of a test well; the drilling results have confirmed the water mixing model.

Received: 20 October 2008 / Accepted: 29 March 2010
Published online: 13 May 2010

D. Boiero · A. Godio (✉)
DITAG – Politecnico di Torino,
C.so Duca degli Abruzzi, 24, 10129, Torino, Italy
e-mail: alberto.godio@polito.it

D. Boiero
e-mail: daniele.boiero@polito.it

M. Naldi
Techgea Servizi SaS,
Via Modigliani, 26/a, 10137, Torino, Italy
e-mail: marionaldi@tin.it

E. Yigit
Uludag Maden Sulari Turk A.S,
Caybasi Koyu, 16370-Osmangazi/Bursa - Turkiye
e-mail: eyigit@uludagicecek.com.tr

Keywords Geophysical methods · Groundwater exploration · Turkey

Introduction

The main purpose of the investigation was to detect promising zones for the location of new wells, through integrated geophysical surveys, so that the company Erbak Uludağ (Uludag, Turkey, Fig. 1) can exploit the mineral water for bottling. The prediction of the hydrogeological layout of the area is of fundamental importance for the proper location of water wells (well siting), for two main reasons: (1) to provide a good discharge rate with a constant chemical composition (particularly important for mineral water bottling); (2) to consider, as much as possible, the natural protection provided by the geologic layout against contaminant filtration.

The main geophysical parameters used in hydrogeological prospecting of a thermally active area are the electrical properties of the geological material. For this reason, the geophysical survey involved the following methods: a time-domain electromagnetic (TDEM) investigation, two-dimensional (2D) electrical resistivity tomography and induced polarisation (ERT-IP) measurements. Particularly, TDEM sounding and electrical-resistivity-tomography yield information on the bulk resistivity of the subsoil, while induced polarisation methods refer to the subsoil polarisability, i.e. the capability to store and release electrical energy of the earth. In the present study, the induced polarisation method is applied in the time domain and the parameter considered is the chargeability.

The combined use of ERT-IP and TDEM methods is well known in thermally active areas (e.g. Pagano et al. 2003) and in general in hydrogeology (Dahlin 1996; Abdul Nassir et al. 2000; Seaton and Burbery 2000; Demanet et al. 2001). Particularly, TDEM prospection has frequently been applied in hydrogeology to map seawater intrusion or to detect freshwater aquifers (Fitterman and Stewart 1986; Fitterman 1987; Hoekstra and Blohm 1990; McNeill 1990; Taylor et al. 1992; Poulsen and Christensen 1999; Sorensen et al. 2001).

In the Uludag area, most of the groundwater circulation has been observed in fractures; an understanding of the interaction between the geophysical parameters and the main geological and hydrogeological features in fractured media is necessary. In such a context, the electrical

 DOI 10.1007/s10040-010-0604-2

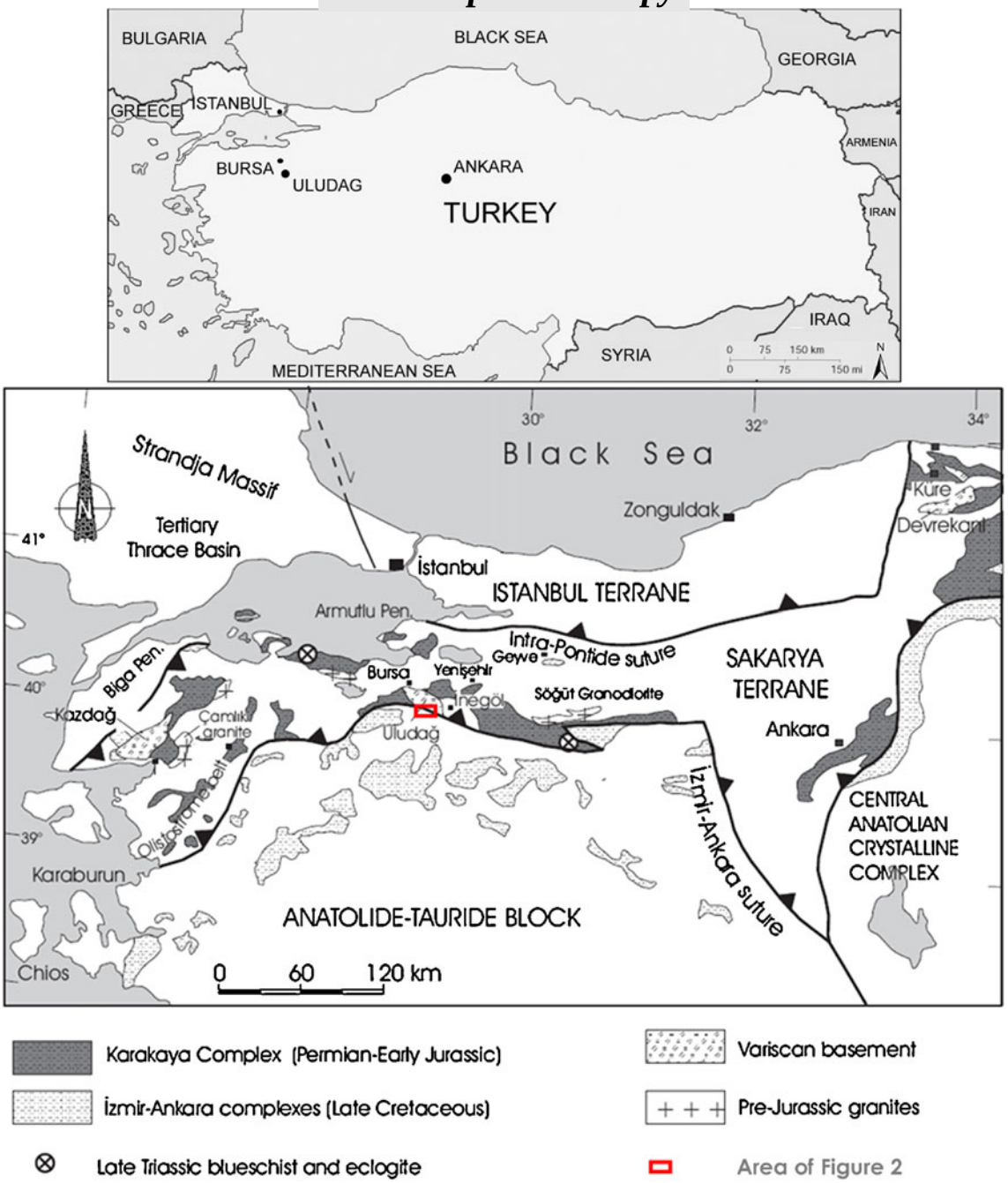

Fig. 1 Geological setting of north-western Turkey; the *red box* refers to the boundary of the area in Fig. 2

resistivity is capable of delineating the main geological units (overburden, metamorphic rocks, etc.), while the water circulation could be more related to the induced polarisation effects.

Resistivity variations in rock mass depend on fracture density and aperture, resistivity of the fluid-filling fractures and pores, and the electrical properties of the rock matrix. In a fractured system, the current conduction is mainly related to the interconnecting pores; the conductivity of pathways is a function of the ionic carriers within the pore fluids, their mobility and the charge of each carrier.

On the other hand, the induced polarisation of fissured rock can be related to the ionic mobility in the interconnected pores. Fredricksberg and Cidarov (1962) suggested that the pore spaces of a rock are composed of successively narrow (active) zones and wide (inactive) zones, which provide an induced polarisation voltage. A relationship between the polarisability and the water-collecting properties of rocks has been established for sandstones and volcanic rocks (Sami Soliman 1970).

The interpretation of the resistivity variations is generally ambiguous and fails to identify individual fracture conduits since low electrical resistivity in a rock

 DOI 10.1007/s10040-010-0604-2

mass can be due to lithology, alteration, or groundwater salinity. In almost all published studies, the resistivity variations associated with hydraulically conductive fracture zones are found to be: (1) difficult to distinguish from similar variations associated with lithological contacts; and (2) attributed to the physical properties of alteration minerals and clay films that line fracture faces rather than hydraulic conductivity (Nelson 1983; Long et al. 1996).

These ambiguities could be reduced if the induced polarisation effect (e.g. the chargeability) is associated with the resistivity data. As a guideline for the data interpretation, the potential zones where mineral water circulates in the rock mass are characterised by low electrical resistivity and high-normalised chargeability values, as suggested by Slater and Lesmes (2002).

According to this, in order to map the most promising zone for the new boreholes, more than 15 TDEM soundings were executed to measure resistivity and 10 applications of electrical tomography were executed to measure resistivity and chargeability (ERT-IP). The TDEM soundings were preferentially aligned along a preset profile with the main goal of obtaining rough information on the geology of the area, while the electrical tomography was distributed throughout the entire area for a more detailed investigation of the presence of groundwater. Finally, only the zones characterised simultaneously by high chargeability and low resistivity values were indicated with a high probability of hosting groundwater.

Area description

The Uludag mineral water plant is located about 30 km south of Bursa (Turkey) in an area of metamorphic rock and tectonic faults (Fig. 2). The ground surface elevation is about 550 m above sea level (a.s.l.). The factory is located at coordinates 40º02′22.00″ N and 29º04′50.00″ E. At present, the bottled mineral water is exploited from two water wells and a spring-source, with a total discharge rate of about 3–4 l/s. Many other water wells have been drilled around the factory, but they remain unused because they are dry or with water, with high concentrations of sodium and borate, that is too mineralised for bottling (deeper water).

Geology

The investigated area is located on a major fault which divides several metamorphic units. There are two main units in the area (Aral et al. 2004; Fig. 2):

1. The "Uludağ complex", a Paleozoic unit made up of a tectonic melange of prevailing granite formation and intruding metamorphic rocks such as schist, marble, amphibolites and gneiss. This unit is located on the north side of the Nilufer fault (Fig. 2);
2. The Karakaia Formation, a Triassic unit composed of serpentine rocks (tectonic slices), limestone and sedimentary rocks (flysch). This unit is located on the left side of the Nilufer valley.

The two geologic units are divided by a major fault which runs along the Nilufer River (see Fig. 3). This major tectonic contact plays a fundamental role in the mineral water rising, as explained better in the following paragraphs. Because of the presence of alluvial deposits (silty-sandy gravel with rounded granite and amphibolites boulders, of a thickness ranging from 3–4 to 15 m), there are only rock outcrops along the river or road cuts in the investigated area.

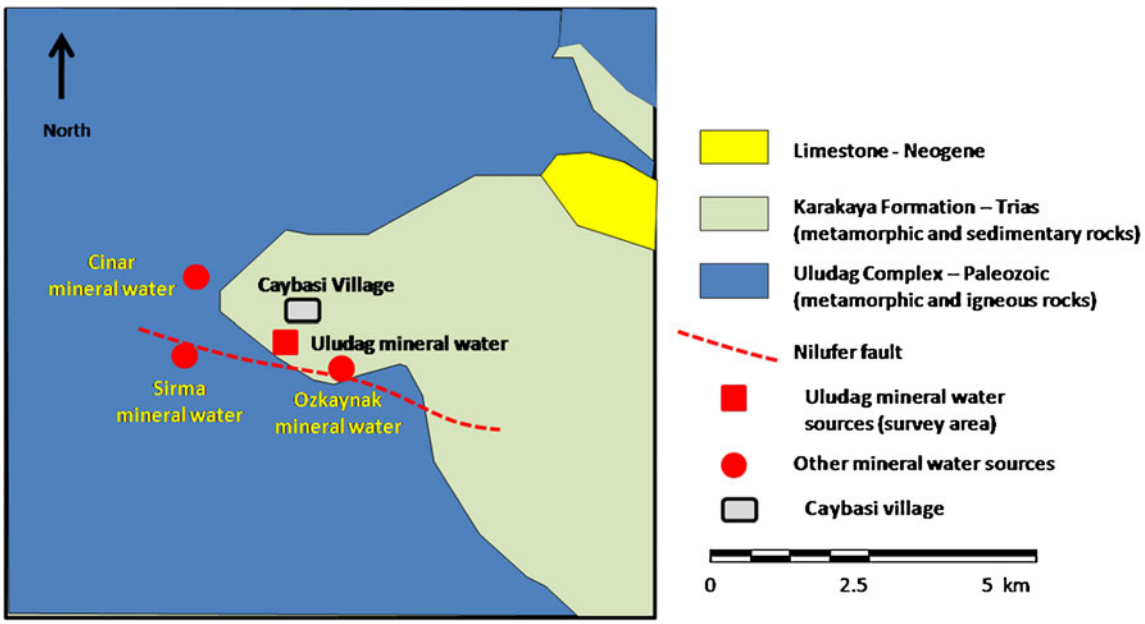

Fig. 2 Simplified geological map of the survey area; the *red box* delineates the survey area (shown in Fig. 3)

DOI 10.1007/s10040-010-0604-2

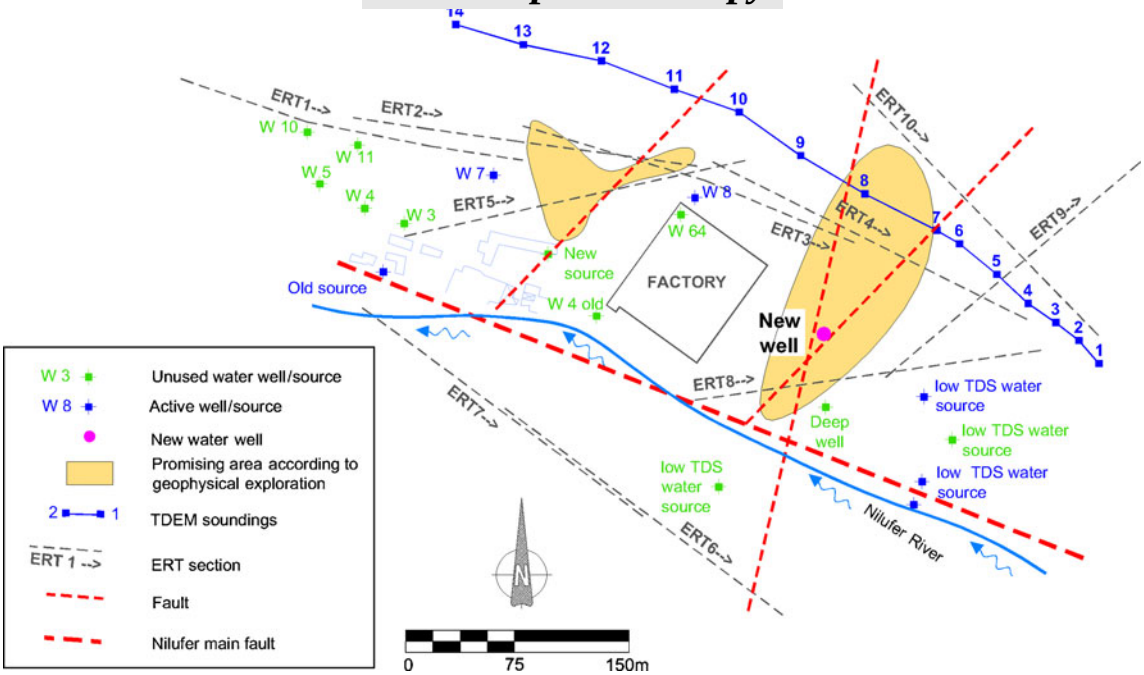

Fig. 3 Sketch map of the survey area with location of the geophysical surveys; the zones indicated as 'promising areas' are the zones that, according to the previous hydrogeological investigations and the geophysical results, have a high probability of being productive

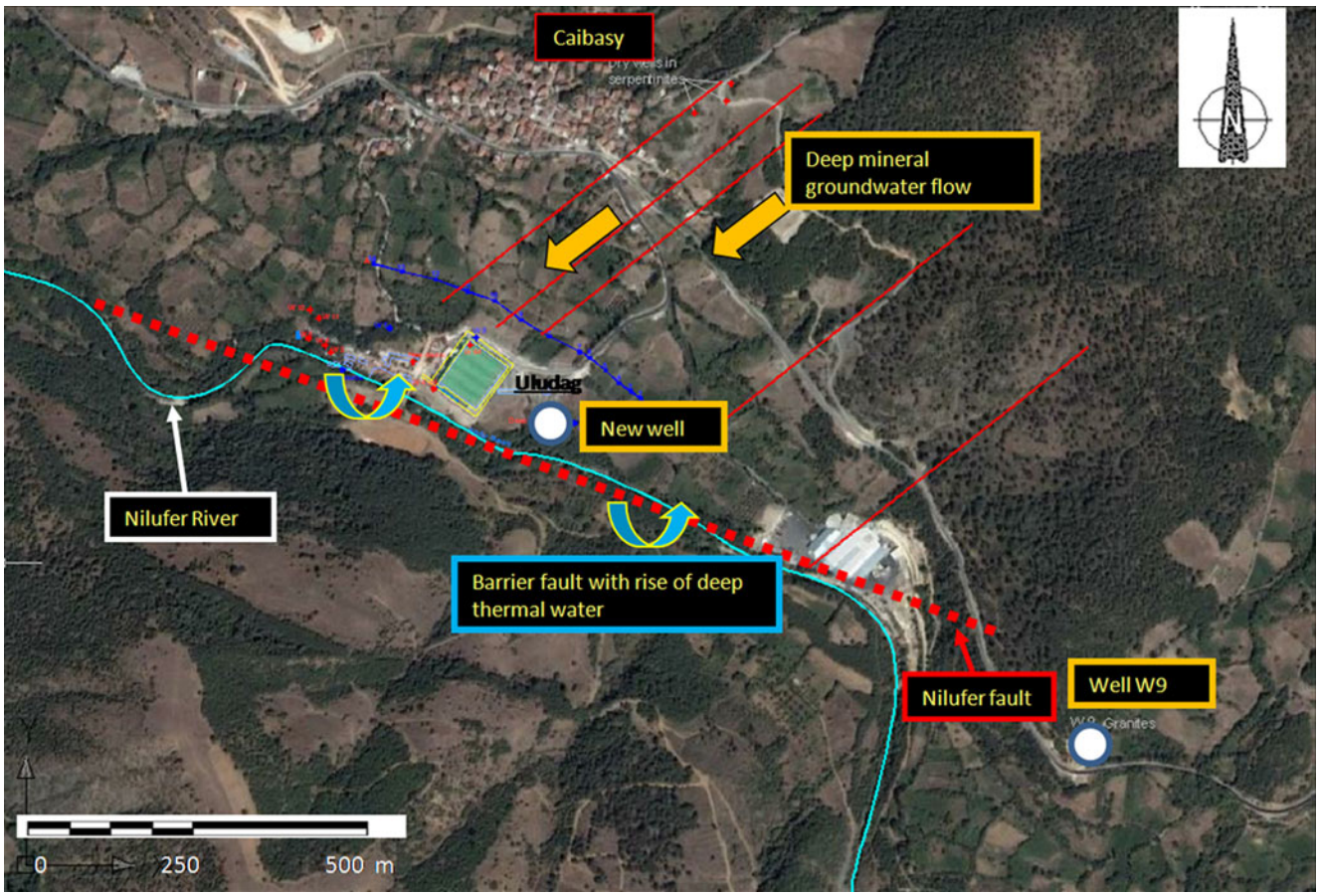

Fig. 4 Sketch map of the survey area with a simplified hydrogeological model

 DOI 10.1007/s10040-010-0604-2

Hydrogeology

There are two aquifers in the studied area (Fig. 4): (1) a shallow aquifer with low mineralised water (the alluvial deposits and the shallow part of the fractured bedrock); the main water well is known as W9, a water well that draws water from a limestone bedrock 1 km from the study area. Chemical analyses of this water (Table 1) have shown a low content of all the parameters, compared to the Uludag bottled mineral water; (2) a very deep aquifer of highly mineralised water, with a deep flow inside fractured granite and serpentine rocks on the right side of the Nilufer River (Figs. 4 and 5). The deep water rises up along the Nilufer fault and has been found in well W64 and in the so-called "deep well" (Fig. 3). Well W64 (no longer active) has highly mineralised water at between 63 and 64 m in depth. The chemical data on this well (Table 1) show a high sodium, chloride and bicarbonate content in the mineral water. The bottled water (W7 and W8) has a lower sodium, chloride and bicarbonate content, and it seems to be diluted, due to the natural mixing of the highly mineralised water and the low mineralised water. The natural mixing between the two "head members" (the W64 and the W9 water) was back calculated with a mass balance fitting (Table 2). The result of the optimised mixed water versus the bottled water shows very few differences, and it matches the hypothesis of natural mixing.

Materials and methods

The time-domain electromagnetic investigation (TDEM) and electrical resistivity (ERT-IP) methods are well known in geophysics exploration and they measure the same fundamental property, resistivity, but have different degrees of sensitivity and do not necessarily respond to the earth in the same manner. TDEM and ERT-IP investigate different depth ranges (usually TDEM can go deeper) and lateral resolutions (TDEM usually provides one-dimensional (1D) vertical soundings, while ERT-IP provides 2D or 3D subsoil images).

In hydrogeophysics, the measurement of soil and rock polarisability is often associated with resistivity data because of its sensitivity to the interface phenomena between fluids and the rock fabric, which can be a sign of the presence of the groundwater. In time-domain surveys, the polarisability of a medium is often expressed by the chargeability, as in the survey here described. When the chargeability is measured together with the resistivity using a tomographic approach, the survey is called 2D or 3D ERT-IP .

The observed electrical parameters

The electrical properties of rock are sensitive to the nature and amount of pore saturant, temperature, and pressure (Llera et al. 1990), surface conduction, and microstructural properties such as porosity of the rock matrix. The amount of the pore saturant and its nature (i.e. whether it is liquid water, other fluids, steam, or other gases) and the microstructural properties are the most significant factors. Most dry rocks are excellent insulators, but saturation with distilled water decreases resistivity by 8 orders of magnitude or even more (Duba et al. 1978). In water-saturated rocks, an increase in temperature from 25 to 250°C decreases the electrical resistivity by about an order of magnitude (Llera et al. 1990). Therefore, the resistivity of intact and fractured rocks is sensitive to the lithology, the temperature, the composition and the state of the pore fluid (Roberts 2001).

For the goal of the present survey (location of faults/fractures with mineral water), polarisability is another significant parameter. As bedrock usually has low polarisability values, the occurrence of mineral water in the subsurface could significantly increase the polarisability parameter along the water-bearing structures (faults or fractures).

Polarisation effects induced by salt water have been discussed by Slater and Lesmes (2002); it is well known that the response of rocks and soils is a function of the lithology and fluid conductivity. Measurements are sensitive to the low-frequency capacitive properties of rocks and soils, which are controlled by diffusion polarisation mechanisms operating at the grain-fluid interface. According to Slater and Lesmes (2002), a parameter that quantifies the magnitude of surface polarisation of the normalised chargeability, is defined as the chargeability divided by the resistivity magnitude. This parameter is proportional to the quadrature conductivity that is measured in the complex resistivity method. For non-metallic minerals, the quadrature conductivity and normalised chargeability are closely related to the lithology (through the specific surface area) and surface chemistry.

Table 1 Main chemical parameters of the available analyses for wells in the shallow (W1, W2, W9 and W10) and deep aquifers (W64)

Water Well	pH	TDS	Na	K	Mg	Ca	Mn	Fe	F	Cl	SO_4	NO_3	HCO_3
W1	6.16	1,354	105	16	62	134	0.14	0.25	1.08	61.44	29	5.72	1,012
W2	6.15	–	51	22	80	159	–	2.7	1.08	80.64	16	5.28	1,171
W64	–	–	509	73	109	437	–	–	–	261	10	8.36	2,976
W7[a]	6.23	–	199	32	84	210	–	–	–	92.5	28.5	0.96	1,269
W8 [a]	5.94	–	79	12	114	211	–	4.79	–	73	15.6	6.64	1,622
W9	–	–	8.92	–	35	45	28.3	29.6	–	14.6	–	0.65	291
W10	–	–	48	–	45	89	–	1.92	–	23.3	29	–	400

[a] Indicates bottled water wells

 DOI 10.1007/s10040-010-0604-2

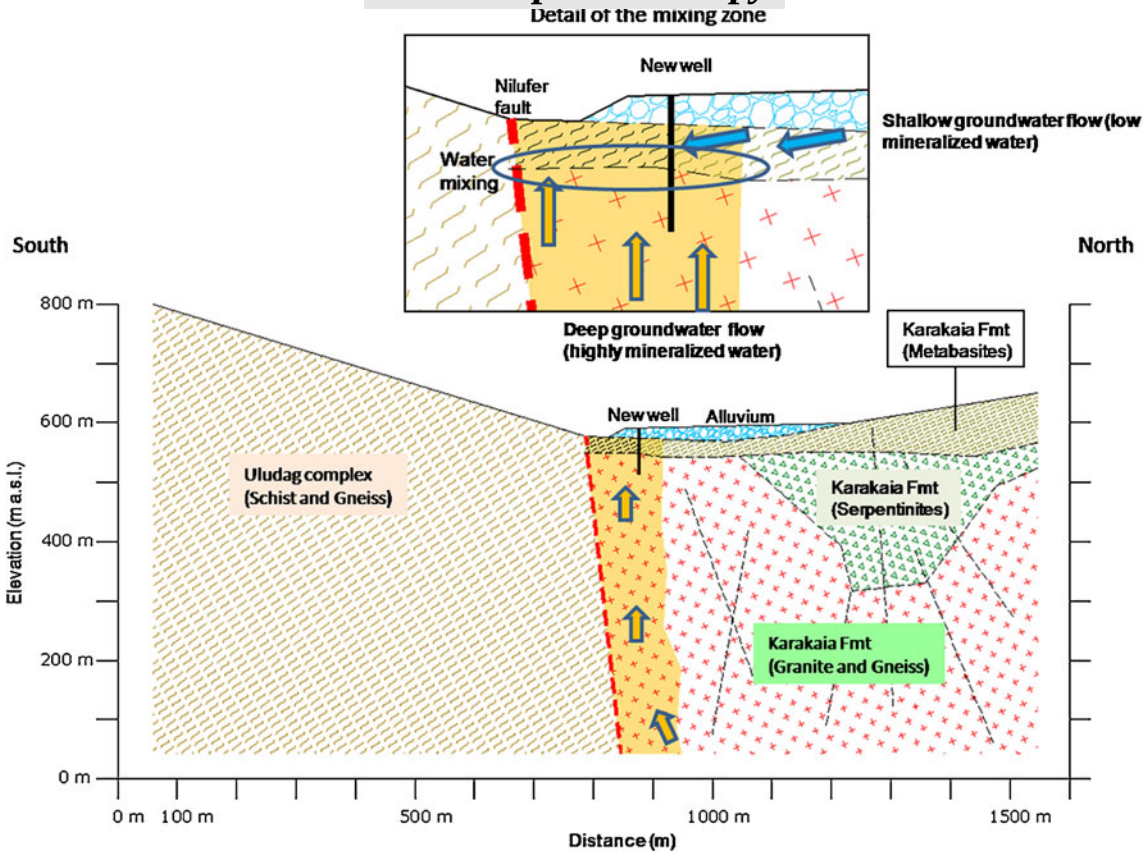

Fig. 5 N–S geological section of the survey area with a simplified hydrogeological model

On the other hand, the chargeability values can be related more to the presence of the water circulation than to the lithology; this is in agreement with the assumption that polarisation occurs in any type of rock, if the surface areas and pore radii are different for the connected pores.

When an electrical current flows through a channel containing pores with different radii (transfer numbers), an excess/loss of ions occurs at the boundaries (Kobranova 1986). The duration of the polarisation process in pores is controlled by the transfer numbers, the radii of the connected pores and the amplitude of the electrical current. If a large pore connects to a narrow pore, the ion concentration in the proximity of the contact decreases. The amplitude of the potential difference depends on many parameters that are constant for the solutions that fill pore spaces: ionic mobility, diffusion coefficient, specific conductivity of the solution, electrical current flowing in the pores, volume of pores and the difference in the transfer numbers.

Time-domain electromagnetic method

The TDEM is based on the propagation of an induced electromagnetic field; a steady current is forced to flow through a loop for some milliseconds to allow a turn-on transient in the ground to dissipate. It is sensitive to conductive units and relatively insensitive to resistive ones.

A time varying magnetic field is created using a coil or loop of wire on the earth surface. Faraday's law of induction tells us that a changing magnetic field will produce an electric field, which in turn will create an electric current. The primary magnetic field from the transmitter loop will create a secondary electric current in the earth. The

Table 2 Calculation of the optimised mixing between the deep water (W64) and shallow water (W9); the mixed water versus the bottled water (W7 and W8) shows very few differences

	Well (deep) W64	Well (shallow) W9	Mixed water [36% (W64)+64%(W9)]	Well (bottled) W7	Well (bottled) W8
Mg (mg/l)	109	35	61	84.0	114.0
Ca (mg/l)	437	45	186	210.0	211.0
Na (mg/l)	509	8.9	189	199.0	79.0
Cl (mg/l)	261	14.6	103	92.5	73.0
HCO_3 (mg/l)	2,976	291	1,257	1,269.0	1,622.0

 DOI 10.1007/s10040-010-0604-2

secondary magnetic field, produced by the induced currents in the earth, is observed at a receiver. The investigated volume by TDEM is a function of the descending and expanding image of the transmitted current, which is usually 20 m × 20 m or greater. The transient of the secondary field is a function of the distribution of the electrical conductivity in the Earth (e.g. McNeill 1990). In principle, TDEM systems can be used to sample very shallow depths. According to this principle, a small transmitter loop was adopted to explore the resistivity at a shallow depth, in the range between a few meters to 100 m.

Electrical resistivity and induced polarisation methods

The resistivity method involves the injection of an electrical current into the ground via electrodes at one or more points and measuring the voltage at several points to calculate the resistivity. Electrical resistivity is calculated as the ratio of the observed electrical voltage versus the injected current, taking into account a geometrical factor, which depends on the mutual distance between the electrodes.

The induced polarisation measurements in the time domain involves the observation of the voltage decay between the two potential electrodes and was observed after the current had been turned off. The voltage decay is usually sampled with a 10-log spaced sampling in the time window of 50 ms to 2 s. The chargeability is computed by integrating the voltage signal decay with respect to the time window; the value was normalised on the voltage values used for the DC resistivity observation.

The apparent chargeability (m) can be expressed (in mV/V) as:

$$m = \frac{1}{V_0} \cdot \int_{t_0}^{t_1} V(t) \cdot dt \qquad (1)$$

where the potential $V(t)$ is integrated in the time window [t0,t1], and divided by the DC potential V_0, used to calculate the apparent resistivity (e.g. Vacquier et al. 1957).

Data acquisition, validation and processing

TDEM

More than 15 TDEM soundings were approximately aligned in a SE–NW direction along a profile (Fig. 3). The spacing between each sounding was 50 m. The adopted Ultra Fast TDEM system permitted the transient decay of the secondary magnetic field to be evaluated, in a coincident square loop configuration with a 50–100 m side, and a maximum output current of 3 A. A ratio of "current on" versus "current off" time of 3/1 and a "current switch off" below 3 ms was adopted. The time window (current off time) extended from 4 μs to 4 ms with 48 signal integration channels. The decay voltage was recorded with a stacking of some hundreds of signals. The normalised voltage (V/I) and the error were given for each channel.

The repeatability of the TDEM data was assessed by using different acquisition configurations (time windows, stacking and amplification); the observed values of the voltage decay with higher errors than 10% were removed from the raw data before the transformation and inversion processing. Fortunately, a low background noise and a good repeatability of the measurements were observed; this allowed only some data to be discharged for higher acquisition times than 1 ms.

The data processing was conducted according to two different strategies. The first one involved the direct transformation (pseudo-gradient transform) of each TDEM signal, which is measured in the normalised potential decay as a function of the time, to retrieve a smoothed 1D vertical resistivity profile. Several schemes have been proposed for direct or approximate analysis of TDEM data (e.g. Nekut 1987; Smith et al. 1994). A simple approximate scheme has been proposed for electromagnetic data analysis by Meju (1998). The scheme transforms the TDEM apparent resistivity data into approximate resistivity-versus-depth information and is a successful adaptation of the Niblett-Bostick transform used in magnetotelluric data analysis (Bostick 1977).

The 2D imaging of TDEM data is usually performed by a kriging procedure of several 1D vertical resistivity profiles, taking into account the anisotropy of the data distribution, where the horizontal resolution is affected by the loop dimension and the station spacing. In order to also take into account the lateral geological effects in the TDEM soundings, a more robust data processing was here performed with the introduction of Laterally Constrained Inversion (LCI; Auken and Christiansen 2004).

Rigorous 1D inversion of the TDEM data is a complex process, even when processing high-quality observed data, because of the non-uniqueness of the solution. To mitigate this problem, each single sounding was inverted, taking into account the information obtained from the closest soundings, according to the approach suggested by Auken and Christiansen (2004). For each model, the unknown parameters were the thickness and the resistivity of each layer.

The data processing is composed of the forward problem, the inversion method and the regularisation. In this case, the forward problem was a central-loop TDEM sounding for different transmitting and receiver square-loop sizes, as proposed by Ingeman-Nielsen and Baumgartner (2006). The inversion method is the linearised least-square inversion scheme and the lateral constraints that act as the regularisation are set between the model parameters of the nearest neighbouring soundings and can be considered as a priori information on the variability of the site geology. The data sets, models, and spatial constraints are inverted as one system. Model parameter information migrates horizontally through the lateral constraints, increasing the resolution of the layers that would be poorly resolved locally. The LCI produces laterally smooth results

 DOI 10.1007/s10040-010-0604-2

with sharp layer boundaries that respect the 2D geological variations of the sedimentary settings.

ERT-IP

In order to investigate the entire area around the factory (the known thermal area and the unknown area), 10 ERT-IP sections were performed, with 48 steel electrodes using a Wenner-Schlumberger array configuration with more than 500 measurements for each section; the length of each section was 235 m (Fig. 3). The resistivity and chargeability data were acquired through an automated controlled resistivity-meter (Syscal Pro, IRIS Instruments, France).

The quality of the resistivity and chargeability data was validated according to the following protocol:

1. In the field, an accurate control of the contact resistance of each electrode was performed, trying to reproduce constant resistance values, but which were, however, no higher than 2 kohm;
2. During the data acquisition, the array-sequence was optimised to minimise the probability of the electrode polarisation effect by avoiding the use of the same electrode that was previously adopted as the current electrode, as the potential electrode, as explained more clearly thereafter;
3. In the data preparation, all the data affected by errors greater than 5%, with respect to the average value of the observed parameter, measured by 3–6 cycles of current injection, were discarded as bad data;
4. In the data processing, the probability distribution of the raw data was analysed to verify whether the probability function fitted a normal or a log-normal distribution; these two probability distribution functions (PDF) are known to be the most recurrent in the statistical analysis of resistivity and chargeability data;
5. Finally, the homogeneity of each distribution function and the similarity between the probability distribution function of the resistivity value and chargeability value were evaluated.

The use of the multielectrode devices should provide some sources of noise in chargeability measurements; in principle they are due to capacitive and inductive effects between transmitter and receiver cables or can be generated by electrode polarisation. The capacitive coupling in the cables is likely to be relatively stable and it decreases quickly with increasing distances between the transmitting cables and the potential reading cables.

In time-domain measurements, it is often assumed that the inductive coupling between the cables via the ground mainly influences the data quality at earlier times and that it quickly decreases; it is convenient to consider the decay curve only after a certain delay (Sumner 1976). To minimise these effects, the voltage decay was integrated starting from a time of 50–100 ms after the current turn-off.

The potential electrodes can be subjected to a charge accumulation if the electrodes have previously been used to transmit a current. In such a case, a strong and much higher potential than the direct current potential itself can take several tens of seconds or some minutes for the charge-up to be discharged. This effect is avoided by using a plus-minus-plus type of injection current cycle (at least 3 cycles); to obtain accurate chargeability measurements, the potential electrodes were only used some minutes after the electrodes had been used to transmit a current (e.g. Dahlin 2000).

Moreover, electrochemical phenomena can provide an additional charge at the potential electrodes (e.g. Vanhala and Soininen 1995); non-polarisable electrodes are therefore usually used. Their use in multielectrode imaging is costly and time consuming: the use of stainless steel electrodes and multicore cables for DC resistivity measurements appears possible, at least in favourable conditions, if particular precautions are taken (Dahlin et al. 2002). The self-potential voltages and the electrode contact resistances were stable and almost constant for each profile, therefore good quality data were guaranteed. The data were inverted through a least squares inversion (L2-norm) software (RES2DINV; Loke 1998), using a resistivity constraint as the lower and upper limits and a finite-element method for the forward modelling process.

Results

The description considers the following two steps: (1) analysis of the section, obtained by TDEM soundings and (2) comparison with the resistivity section which overlaps the TDEM section. These steps provide an overview of the main geological and hydrogeological features of the area, while the description of the vertical sections of ERT-IP offers a more detailed scenario of the relationship between the geophysical response and the hydrogeological model.

The TDEM results are plotted in terms of 2D vertical sections of the resistivity obtained by the pseudogradient transform and by the laterally constrained inversions (Fig. 6). The two sections depict the following main features:

- The most conductive zone is between the soundings 9 and 13, NW of the factory, where most of the water wells are located; the conductive zone is upper delimited by a most resistive limit (clearly depicted in the soundings 11–14), which separates the thermal water from the freshwater that circulates in the shallow part of the section, inside the alluvial deposits, and shallow granites or sedimentary rocks;
- On the eastern part of the sections, the uppermost layers are characterised by low resistivity values (10–15 ohm m), above a more resistive bedrock (80 ohm m).

It appears evident, particularly in the pseudo-gradient section, how the resistivity distribution changes from west towards east, probably indicating the presence of a significant fault. From a geological point of view, the

 DOI 10.1007/s10040-010-0604-2

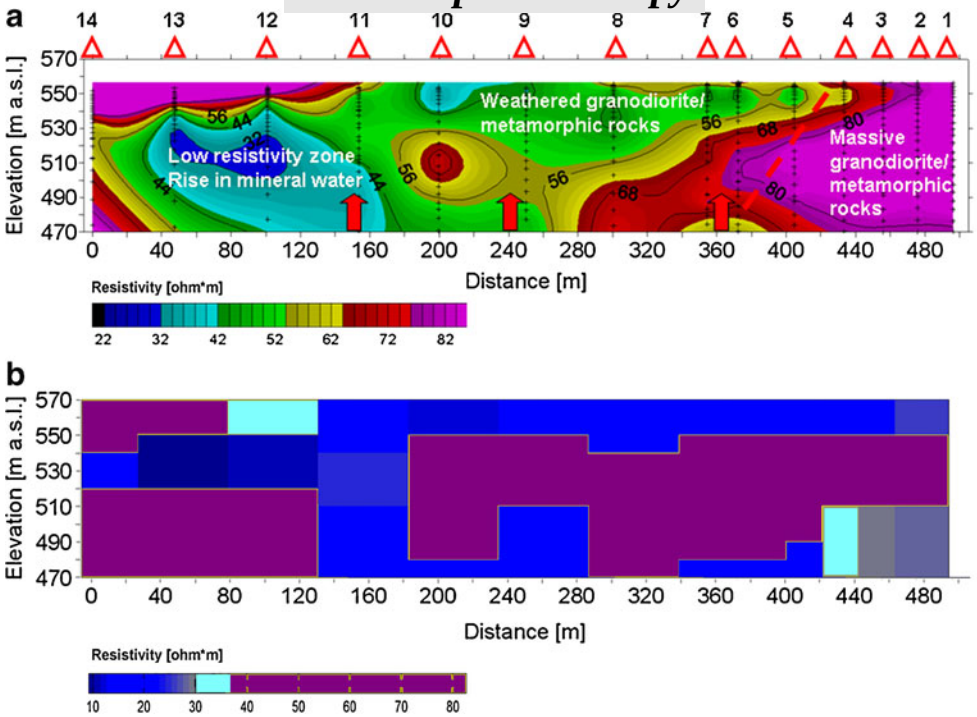

Fig. 6 TDEM resistivity sections (west is on the *left side*); **a** interpolated section after applying a 1D pseudo-gradient transform to each sounding (see text for explanation); **b** Laterally constrained inverted section

TDEM section has defined two different structural blocks. The resistive block on the eastern side, according to the calibration of the "deep water well", is mainly made up of a serpentine lens surrounded by sedimentary rocks (mainly flysch). There is a clear conductive zone on this block (quite deep) within a deep thermal-water-bearing fault. This water is intercepted by the deep water well (the exact depth of the water inflow in the well is unknown). The more conductive block in the western part of the section is made up of fractured granite; the stratigraphy of the water wells is unknown but the presence of granite was confirmed in the drilling operations.

A simplified geological and hydrogeological interpretation of the TDEM section, after the calibration of the geophysical response by the stratigraphic evidence, is summarised as follows:

- In the western part of the section, the low resistivity at the elevation of about 530 m could be related to the main rise of the mineral water;
- In the central part of the section, the near surface layer, characterised by intermediate/low resistivity values, refers to the presence of weathered granodiorite and altered metamorphic rock;
- The high resistivity values, pointed out in the eastern part of the section at elevation below 530 m, are consistent with the presence of massive granodiorite and more compact metamorphic rock.

Statistical analysis of the results of resistivity and chargeability data enabled assessment of the data quality; the probability distribution function (PDF) of the experimental data was used to show evidence of data trends and the presence of "spikes" that can be related to noise, as opposed to the spikes related to geological and hydrogeological features. The step is particularly relevant in the analysis of the chargeability data, where the sensitivity to noise is usually very high: a regular distribution of the observed apparent chargeability data is necessary in order to obtain a realistic inverted model (section of the real chargeability); usually a non-regular distribution of the chargeability data provides a great negative interference in the quality and reliability of the final solution (chargeability sectons).

The results of the PDF of ERT-IP 2 are here described (Fig. 7). The experimental data set is made up of more than 500 apparent resistivity measurements and apparent chargeability values. The PDF of the resistivity data matches a normal distribution, while the chargeability seems to match a log-normal distribution. The median values of the apparent resistivity data are around 50 ohm m with only a few values above 100 ohm m. The chargeability distribution shows a high number of data values in the range between 2–5 mV/V, while for upper values, the distribution shows a regular trend with a gentle decreasing of the data population with the increasing of the chargeability values. This regular trend refers to a homogeneous background of the chargeability with numerous data that are mainly associated with consistent chargeability anomalies related to subsoil response.

The inverted sections ERT-IP 2, ERT-IP 4 and ERT-IP 8 are shown in Figs. 8, 9 and 10, respectively. The sections show the distribution (contour model) of the resistivity (ohm m) and the chargeability (mV/V) along

 DOI 10.1007/s10040-010-0604-2

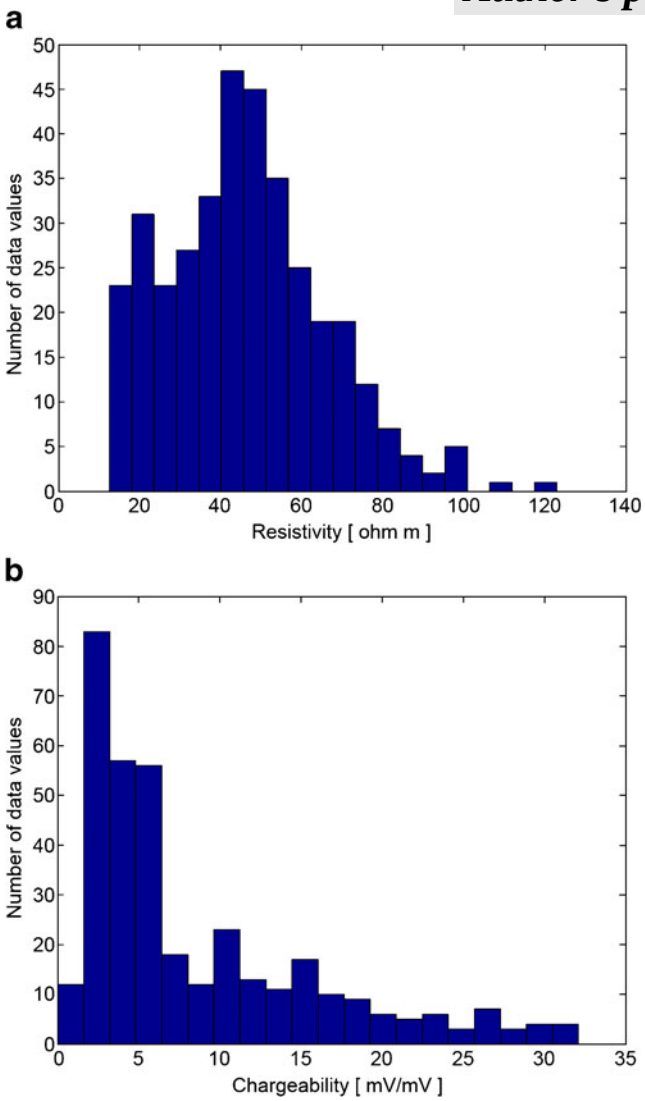

Fig. 7 Examples of data distribution of apparent resistivity and chargeability values of electrical tomography, line 2; **a** the resistivity distribution tends to a normal distribution while **b** the chargeability data are characterised by a log-normal distribution

vertical planes. The sections point out a rather regular stratigraphic interface between the uppermost electrically conductive layer (10 ohm m), which is mainly characterised by clay soil that overlies a more resistive horizon, here ascribed as metamorphic rock.

On the right side of the Nilufer valley, in the area west of the factory, four tomographic sections were traced (profiles 1, 2, 3 and 5). The results indicate the presence of a hot spot of chargeability response in the area located between well 7 and well 8. The anomaly was found in ERT-IP 5 and ERT-IP 2 (see their location on Fig. 3); this feature identifies a promising zone for the drilling of new wells. Another anomaly of the chargeability response is located between well 11 and well 7.

The results of the ERT-IP sections, located on the right side of the Nilufer valley, in the area east of the factory (profiles 4, 8, 9 and 10), indicate a possible occurrence of mineral water along a lineament running from the deep well to the access road. As shown in ERT-IP section 8 (Fig. 10), a chargeability anomaly was detected very close to the deep well. This anomaly was also found (with lower intensity) in ERT-IP 4 and in ERT-IP 9. On the other hand, the ERT-IP 10 section does not show any evidence of chargeability anomaly. For this reason, it can be assumed that the mineral water does not flow north of the ERT-IP 4 line.

The TDEM interpretation allows one to estimate the main conductive and resistive zone to a depth of 100 m, permitting the information pointed out by the ERT-IP sections to be extended to a deeper level. A comparison of the depth of investigation of the two methods is depicted in Fig. 11, where the electromagnetic section, obtained from the direct transform of each single TDEM sounding, is compared with the electrical resistivity tomography, which overlaps the TDEM image in its final part. It can be noted as the electromagnetic section shows a more gradual increase in the resistivity with the depth, the low resolution of the TDEM section does not permit an accurate estimate of the depth of the interface between the clay material and the serpentine rocks. This interface is more clearly detected in the resistivity section of the ERT-IP.

Discussion

The limits and validity of the results, taking into account the ambiguities of the different interpretation processes, are discussed. Then a hydrogeological interpretation of the main results is given.

The achieved results are consistent with the basic concepts of the electrical response in weathered crystalline rocks. The rocks in the surface zone are moderately good conductors of electricity, because they contain relatively large amounts of water in the pore spaces and other voids. This zone has resistivity values that vary from about some tens of ohm m, in recent sediments, to 1,000 ohm m or more in weathered crystalline rock. Since most rock-forming minerals are good insulators at normal temperatures, the conduction of electricity in such rocks is determined almost entirely by the water they contain. The common drawback in the interpretation of the geophysical survey is the inherent ambiguity that results when zones of anomalous response are related to changes in fracture permeability, but this ambiguity could also be attributed to alteration, rock texture, or lithology. A joint analysis of resistivity and chargeability data could minimise the ambiguity.

The most electrically conductive zone is between the TDEM soundings 9 and 13, NW of the factory, where most of the water wells are located. The conductive zone is upper delimited by a sort of hydrogeological limit, which separates the thermal water from the freshwater that circulates in the shallow part of the section, inside the alluvial deposits, and shallow granites or sedimentary rocks. The mixing of deep water and shallow freshwater occurs along faults or fractured zones, where deep water outflows can reach the surface or the shallow part of the subsoil. The most productive well (W7) is located just above one of these outflows.

 DOI 10.1007/s10040-010-0604-2

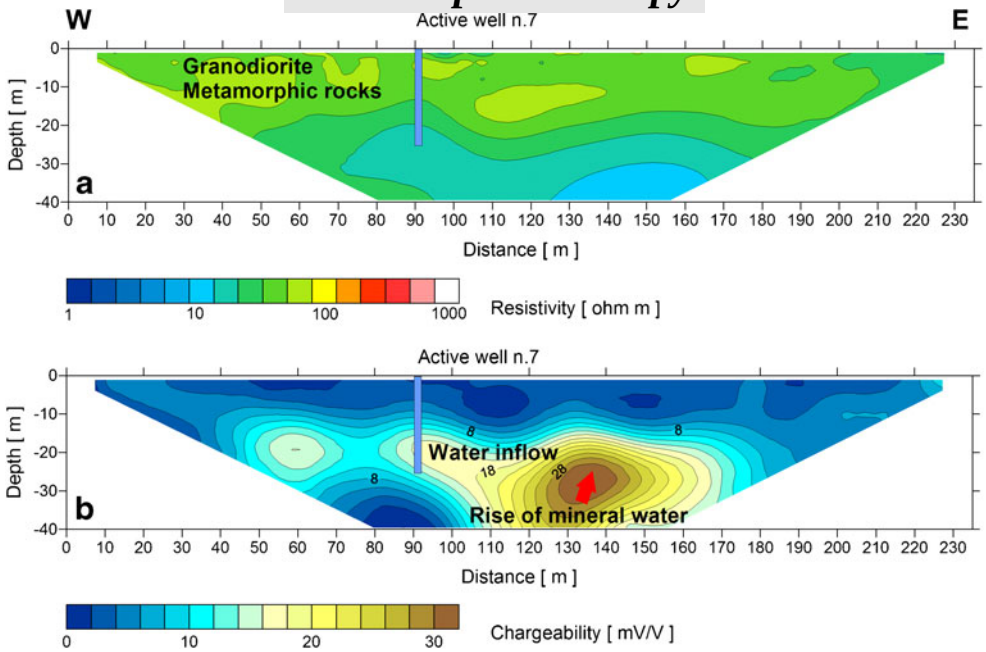

Fig. 8 **a** Electrical resistivity tomography and **b** chargeability section line 2

The circulation of mineral (high salinity) water within the main fractures provides a polarisability of the region, which is subject to high tortuosity, where ionic charges can accumulate in the narrow pores and the current is released when the external electrical field is removed.

In an attempt to relate the results of the resistivity and chargeability section in order to detect the most permeable zone in the massive rocks, the chargeability response was normalised with respect to the observed resistivity values. This approach permitted the main resistivity gradients to be associated with the anomalies in the chargeability response (Fig. 12). The effect is two fold: it reduces the ambiguities of the interpretation of the single parameter distribution and points out the chargeability hot spots that were not associated with a gradient of the resistivity distribution. In such a way, the effect of the main "ghosts" or pitfalls in the interpretation of the chargeability data were minimised in the formulation of the hydrogeological model.

The distribution of the chargeability values normalised on the resistivity was computed (e.g. line 2) and plotted in Fig. 12. This plot enhances the effect of the electrical response that is indicated at the bottom of the section and validates the hypothesis that the water circulation from a

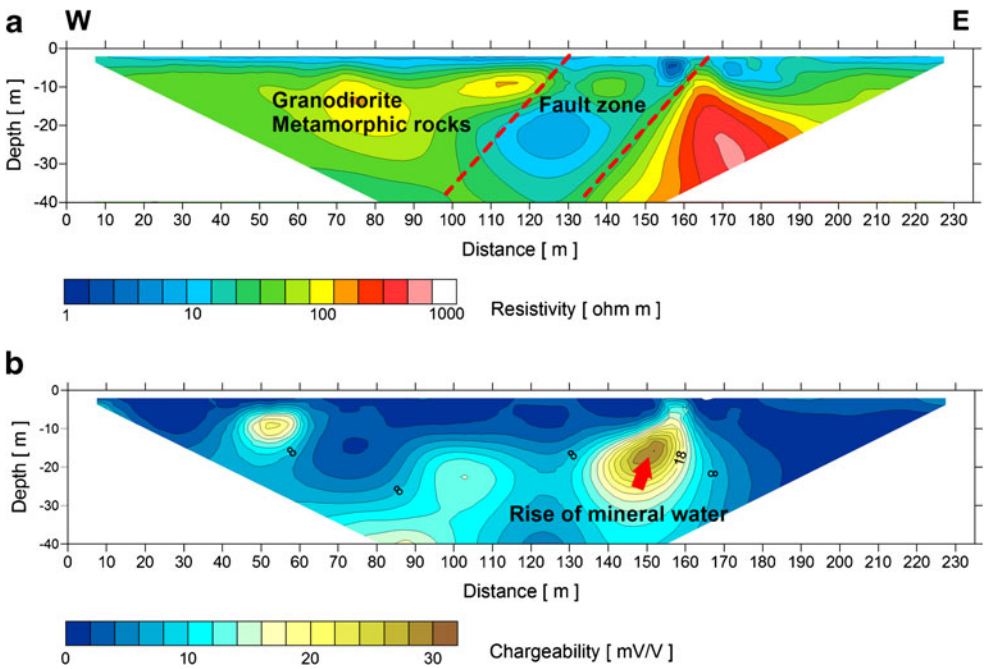

Fig. 9 **a** Electrical resistivity tomography and **b** chargeability section (mV/V), line 4

 DOI 10.1007/s10040-010-0604-2

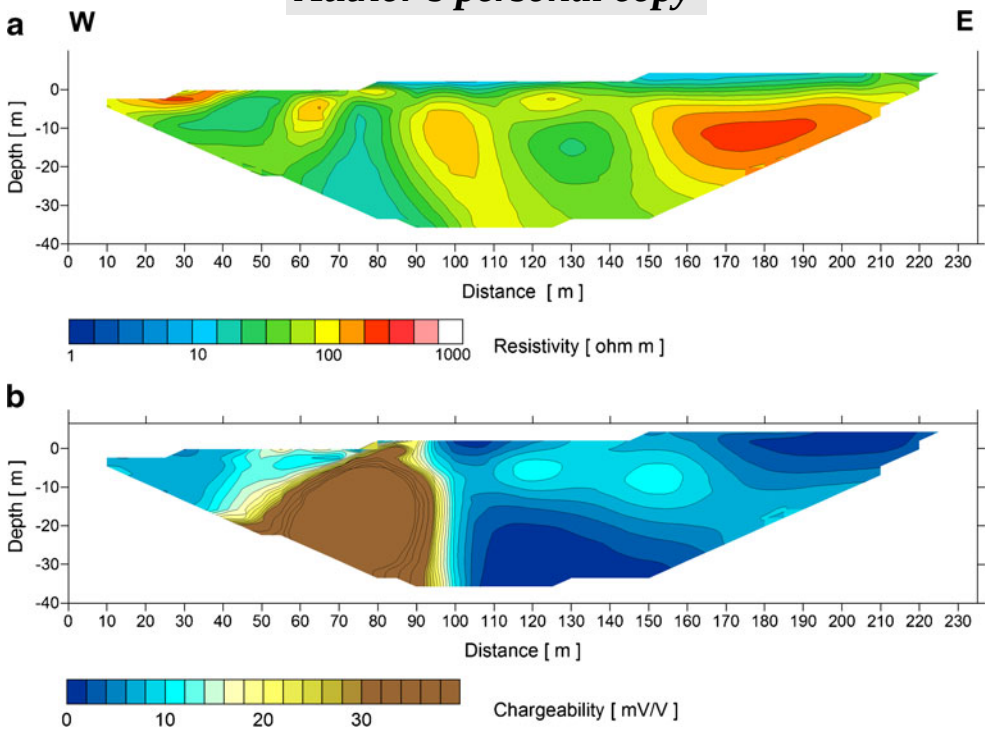

Fig. 10 **a** Electrical resistivity tomography and **b** chargeability section (mV/V), line 8

deeper level is responsible for the chargeability anomaly in the presence of a resistivity value gradient. This interpretation is based on the analysis of the most effective zone where the chargeability value peak corresponds to the significant decrease in resistivity. This section enabled minimisation of the importance of the chargeability anomaly located at the 60 m coordinate, which was detected by the analysis of the chargeability section only and which is probably due to some "ghost" effects.

As far as section 4 (Fig. 9) is concerned, the chargeability/resistivity ratio plot (Fig. 12) enhances the effect of the more permeable zone (fault zone?)

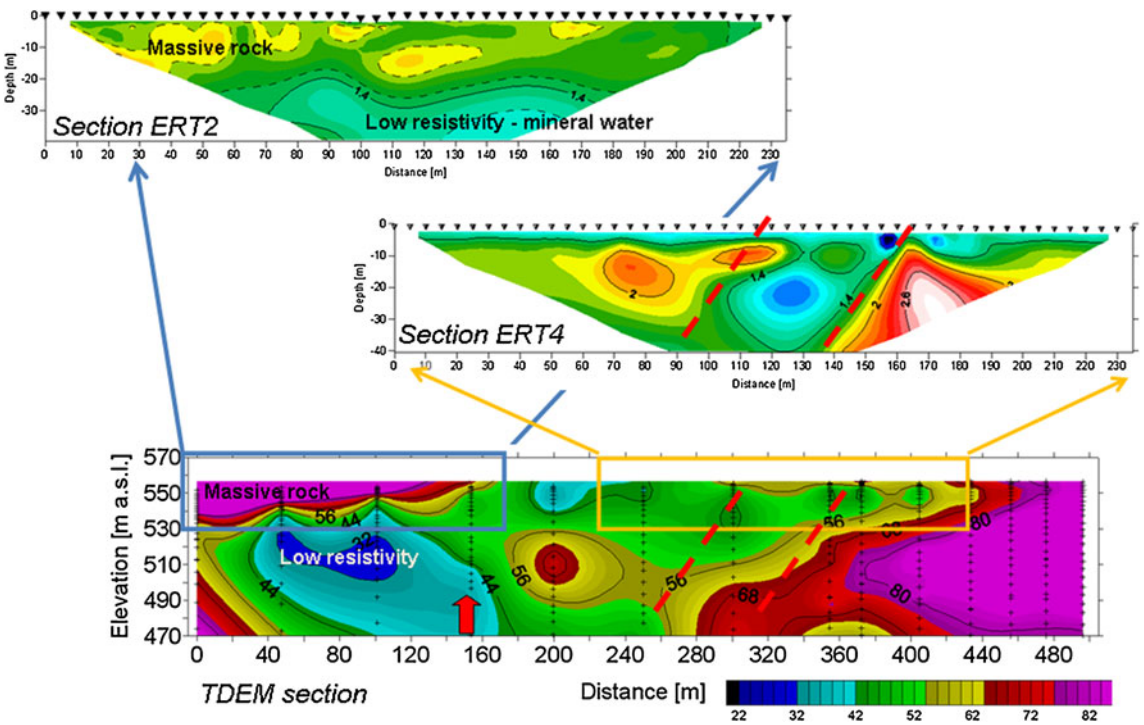

Fig. 11 Partial overlap of the TDEM section and the electrical resistivity tomography of lines 2 and 4; the resistivity values of tomographic sections are in logarithmic scale (ohm m)

 DOI 10.1007/s10040-010-0604-2

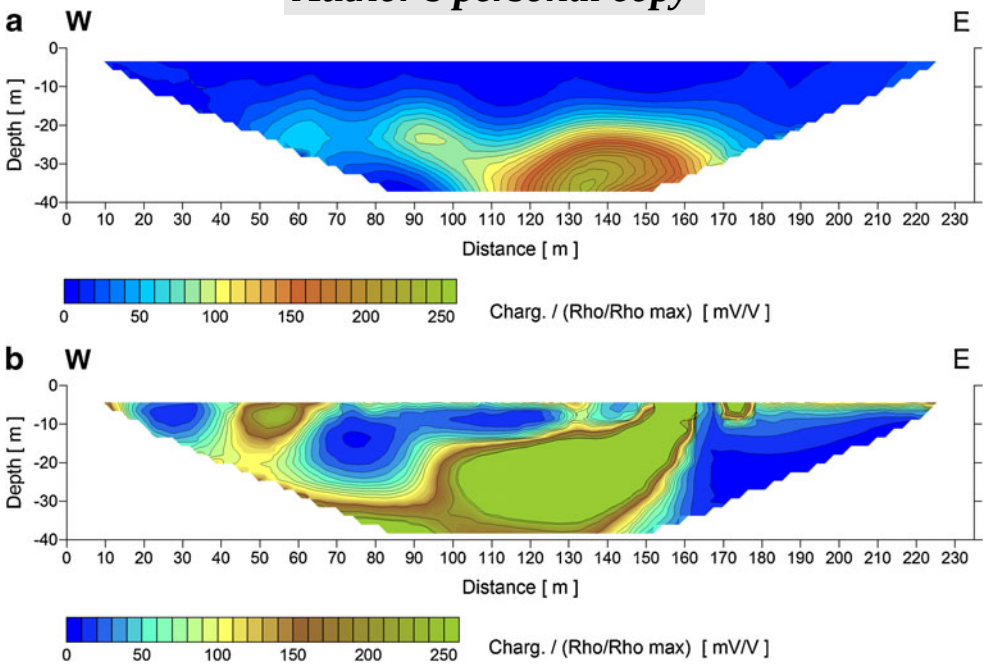

Fig. 12 Ratio of the chargeability values with respect to the normalised resistivity values; **a** line 2; **b** line 4

where the presence and circulation of mineral water should affect the electrical behaviour of the rock mass. Moreover, an intense near-surface anomaly is clearly pointed out; this probably characterises an intense circulation of the surficial groundwater.

As the electrical resistivity of the water samples, collected at the different wells, ranges from 2 to 6 ohm m (at a reference temperature of 25°C) from the deeper wells up to the uppermost water inflow, it is evident that the water circulation affects the resistivity of the hosting rocks to a great extent. These low resistivity values are related to the salts dissolved in the water, which can be divided into positively and negatively charged ions. The contribution in the electrical conductivity of water is mainly due to the major positively charged ions such as sodium 3 (Na+), calcium (Ca^{+2}), potassium (K^{+}) and magnesium (Mg^{+2}). The major negatively charged ions are chloride (Cl^{-}), sulphate (SO_4^{-2}), carbonate (CO_3^{-2}), and bicarbonate (HCO_3^{-}). Nitrate (NO_3^{-2}) and phosphate (PO_4^{-3}) contribute less to conductivity, although they are very important biologically. Laboratory tests at high temperatures (Llera et al. 1990) have pointed out that the electrical resistivity of rocks depends on the fluid saturation and on the fracture properties of the rock matrix and on the chemical reactions between the pore electrolytes and the minerals. Moreover, electrical conductivity is highly temperature dependent. Electrolyte conductivity increases with temperature at a rate of 0.0191 mS/m°C for a standard KCI solution of 0.0100 mol. For natural waters, this temperature coefficient is only approximately the same as that of the standard KCI solution. Thus, the more the sample temperature deviates from 25°C, the greater the uncertainty in applying the temperature correction. According to the high salt contents of water-bearing fractures and the temperature effect, it was expected that the values of the geological horizons involved in water circulation would be in a range of 10–30 ohm m.

On the basis of the results of the geophysical survey, two promising zones were identified (see Fig. 4): the first is located between well W7 and W8 (the active wells), while the second is located outside the factory area, along a secondary fault. Both selected areas show high chargeability values and low resistivity, which could be related to the occurrence of mineral water circulation.

A well was drilled in one of the promising zones (the second zone; the first promising zone was discarded to avoid interference with active wells W7 and W8) to test the water. The test well has been labelled “new well” in Fig. 3. The well is close to the anomaly, pointed out in the section ERT-IP 8, and characterised by chargeability values above 30 mV/V and resistivity lower than 10 ohm m (Fig. 10). As reported in the log stratigraphy of Fig. 13, the new well (drilled with the air-lift method without core-recovery) encountered a first part of loose sediments (0–22 m), then a sequence of metamorphites (22–46 m) and gneiss/granite (46–75 m).

Five water inflows were detected. The first water inflow is located inside the shallow bedrock at 34 m in depth. The groundwater has a low electrical conductivity (about 0.5 mS/cm at 25°C) and a discharge rate of about 0.5 l/s, and can be classified as “shallow water” and it is indicated as water A (Fig. 13). The following inflows (second and the third) are indicated as water A+B and are located in red granite, at a depth of 46 and 51 m. Because of the risk of well collapse, the fractures were not insulated with a packer system, and it was only possible to measure the increase in the electrical conductivity (about 1.3 mS/cm) and in the total discharge rate of about

 DOI 10.1007/s10040-010-0604-2

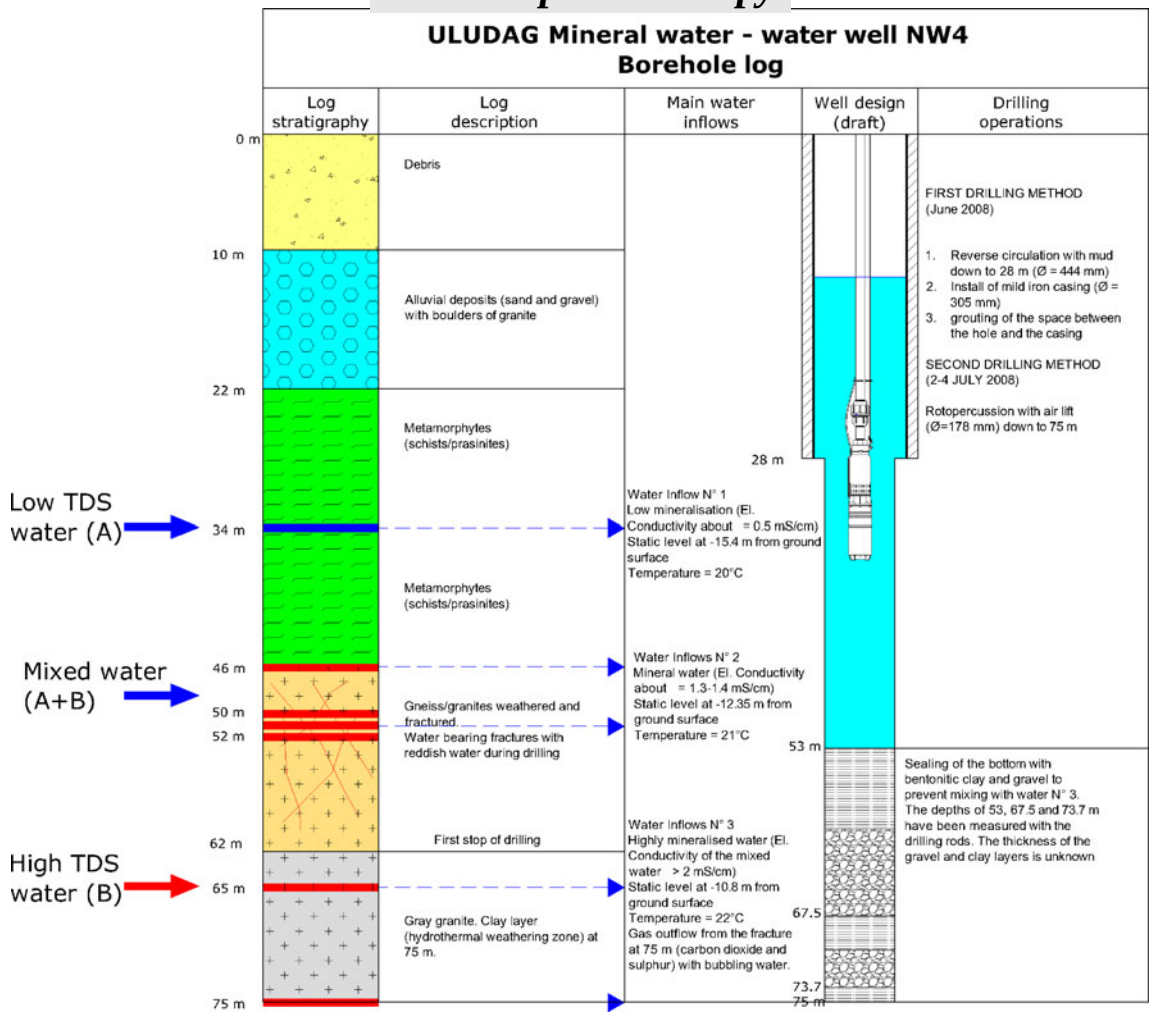

Fig. 13 Stratigraphic column of the new well; the *bold lines* refer to the groundwater inflow at different levels: the *blue arrows* indicate low total dissolved solids (TDS) water, while the *red arrow* indicates higher TDS water

1.2–1.4 l/s. At a depth of 62 m, a layer of highly weathered granite (clayey weathering probably due to hydrothermal activity) was encountered and then grey granite with two more water-bearing fractures. The water yield increased to 2–2.5 l/s, and the electrical conductivity also increased to value greater than 2 mS/cm (indicated as water B). In addition, the new water was "bubbling" due to the presence of gas (carbon dioxide) and smelling of "rotten eggs" (hydrogen sulphide); all these "signs" indicate that this new water is highly mineralised. The bottom of the well was then closed and the two water-bearing fractures were sealed in order to monitor the mineral water and its suitability for bottling.

Conclusions

A geophysical survey using combined methods (TDEM and ERT-IP) has been applied for a well siting in a complex hydrothermal area in Turkey (Uludag area). The successful characterisation of the fractured-bedrock aquifers, at the site scale, requires the effective integration of different geophysical and hydrogeological tools. The TDEM survey permitted an overview of the resistivity distribution to the depth of about 100 m. The data were calibrated with the well stratigraphy in order to associate the range of electrical resistivity with the main geological units. The joint analysis of the resistivity and chargeability sections is more promising for delineating the presence of groundwater circulation.

It was found that resistivity values are more sensitive to rock lithology and alteration, while chargeability is sensitive to the dynamic effects (water circulation). This fusion of resistivity and chargeability data confirmed the presence of two promising zones. The results of the new drilling in one of the two areas provided a great deal of information concerning the hydrogeological model of the thermal area, which can be summarised as follows: (1) the test well found mineral water with a good discharge rate (1.5–2 l/s) compared to all the other existing wells and

 DOI 10.1007/s10040-010-0604-2

considering that it was from a fractured aquifer in granite; this means that the geophysical anomalies could be related to the mineral groundwater circulation (probably along the water-bearing faults/fractured zones); (2) different types of water have been encountered in the well, from more shallow freshwater to deeper, highly mineralised water. The mineral water suitable for bottling is clearly the result of a natural mixing of shallow freshwater and deep highly mineralised water. It is also clear that the water wells cannot be drilled any deeper than 45–50 m because the deep (saline) water would prevail over the freshwater and, in such a case, the values of the chemical parameters of the mixed water would render it no longer useable for mineral drinking water purposes.

Acknowledegments We highly appreciated the competence and the availability of Maria-Th. Schafmeister (Editor) and Susanne Schemann and Sue Duncan (Editorial Office); we are also grateful to two anonymous reviewers for their suggestions and comments, which improved the quality of the manuscript.

References

Abdul Nassir SS, Loke MH, Lee CH, Nawawi MNM (2000) Salt-water intrusion mapping by geoelectrical imaging surveys. Geophys Prospect 48:647–661

Aral Ü, Okay M, Cemal G, Oùlu NC (2004) The Karakaya Complex: a review of data and concepts. Turkish J Earth Sci 13:77–95

Auken E, Christiansen AV (2004) Layered and laterally constrained 2D inversion of resistivity data. Geophysics 69:752–761

Bostick FX (1977) A simple almost exact method of MT analysis. Workshop on Electrical Methods in Geothermal Exploration, Snowbird, Utah, 1976, contract no. 14080001-8-359, US Geological Survey, Reston, VA

Dahlin T (1996) 2D resistivity surveying for environmental and engineering applications. First Break 14:275–283

Dahlin T (2000) Electrode charge-up effects in DC resistivity data acquisition using multielectrode arrays. Geophys Prospect 48:181–187

Dahlin T, Leroux V, Nissen J (2002) Measuring techniques in induced polarisation imaging. J Appl Geophys 50:279–298

Demanet D, Renardy F, Vanneste K, Jongmans D, Camelbeeck T, Megrahoui M (2001) The use of geophysical prospecting for imaging active faults In the Roer Graben, Belgium. Geophysics 66:78–89

Duba A, Piwinskii AJ, Santor M, Weed HC (1978) The electrical conductivity of sandstone, limestone and granite. Geophys J R Astron Soc 53:583–597

Fitterman DV (1987) Examples of transient sounding for ground water exploration in sedimentary aquifers. Ground Water 25:685–692

Fitterman DV, Stewart MT (1986) Transient electromagnetic sounding for groundwater. Geophysics 51:995–1005

Fredricksberg DA, Cidarov MP (1962) Study of the relation between induced polarization phenomena and the electrokinetic properties of the capillary system (in Russian). Vestnik of the Leningrad Univ. 4, Geophysics and Chemistry Series

Hoekstra P, Blohm-mW (1990) Case histories of time-domain electromagnetic soundings in environmental geophysics. Geotech Environ Geophys 2:1–15

Ingeman-Nielsen T, Baumgartner F (2006) CR1Dmod: a MATLAB program to model 1D complex resistivity effects in electrical and electromagnetic survey. Comput Geosci 32:1411–1419

Kobranova VN (1986) Petrophysics (in Russian). Nedra, Moscow

Llera FJ, Sato M, Nakatsuka K, Yokoyama H (1990) Temperature dependence of the electrical resistivity of water-saturated rocks. Geophysics 55:576–585

Loke MH (1998) Rapid 2D resistivity and IP inversion. Geotomo Software, Penang, Malaysia

Long JCS, Aydin A, Brown SR, Einstein HH, Hestir K, Hsieh PA, Myer LR, Nolte KG, Norton DL, Olsson OL, Paillet FL, Smith JL, Thomsen L (1996) Rock fractures and fluid flow: contemporary understanding and applications. National Academy Press, Washington, DC, 551 pp

McNeill JD (1990) Use of electromagnetic methods for groundwater studies. Geotech Environ Geophys 1:191–218

Meju MA (1998) A simple method of transient electromagnetic data analysis. Geophysics 63:405–410

Nekut AG (1987) Direct inversion of time-domain: electromagnetic data. Geophysics 52:1431–1435

Nelson HR (1983) New technologies in exploration geophysics. Gulf, Houston, Texas

Pagano G, Menghini A, Floris S (2003) Electrical tomography and TDEM prospection in the Chianciano thermal basin (Siena, Italy). Annals Geophys 46:501–512

Poulsen LH, Christensen NB (1999) Hydrogeophysical mapping with the transient electromagnetic sounding method. Eur J Environ Eng Geophys 3:201–220

Roberts JJ (2001) Electrical properties of microporous rock as a function of saturation and temperature. J Appl Phys 21:1687–1694

Sami Soliman M (1970) Induced polarization, a method to study water-collecting properties of rocks. Geophys Prospect 18:654–665

Seaton WJ, Burbery TJ (2000) Aquifer characterization in the Blue Ridge physiographic province using resistivity profiling and borehole geophysics: geologic analysis. J Environ Eng Geophys 5:45–58

Slater LD, Lesmes D (2002) IP interpretation in environmental investigations. Geophysics 67:77–88

Smith RS, Edwards RN, Buselli G (1994) An automatic technique for presentation of coincident loop, impulse-response, transient electromagnetic data. Geophysics 59:1542–1550

Sorensen KI, Efferso F, Auken E (2001) A hydrogeophysical investigation of the island of Drejo. Eur J Environ Eng Geophys 6:109–124

Sumner JS (1976) Principles of induced polarization for geophysical exploration. Developments in Economic Geology, vol 5. Elsevier, Amsterdam, 277pp

Taylor K, Widmer M, Chesley M (1992) Use of transient electromagnetics to define local hydrogeology in an arid alluvial environment. Geophysics 57:343–352

Vanhala H, Soininen H (1995) Laboratory techniques for measurement of spectral induced polarization response of soil samples. Geophys Prospect 43:655–676

Vacquier V, Holmes CR, Kintzinger PR, Lavergne M (1957) Prospecting for groundwater by induced electrical polarisation. Geophysics 23:660–687

 DOI 10.1007/s10040-010-0604-2